FIRST PRINCIPLES STUDY OF ELECTRONIC AND OPTICAL PROPERTIES OF PRISTINE AND X (Cu, Ag AND Au) DOPED BiOBr

S. Paudel, P. R. Adhikari, O. P. Upadhyay, G. C. Kaphle and A. Srivastava

Journal of Institute of Science and Technology

Volume 22, Issue 2, January 2018

ISSN: 2469-9062 (print), 2467-9240 (e)

JIST, **22** (2): 63-69 (2018)

Published by:

Institute of Science and Technology

Tribhuvan University

Kirtipur, Kathmandu, Nepal

JIST 2018, 22 (2): 63-69
ISSN: 2469-9062 (p), 2467-9240 (e)

Research Article

FIRST PRINCIPLES STUDY OF ELECTRONIC AND OPTICAL PROPERTIES OF PRISTINE AND X (Cu, Ag AND Au) DOPED BiOBr

Samir Paudel[1], Puspa Raj Adhikari[1,3], Om Prakash Upadhyay[1], Gopi Chandra Kaphle[2,4,5*], Anurag Srivastava[3]

[1]Patan Multiple Campus, Tribhuwan University, Lalitpur, Nepal
[2]Central Department of Physics Tribhuvan University, Kirtipur, Nepal
[3]ABV- Indian Institute of Information Technology and Management, Gwalior, India
[4]Condesed Matter Physics Research Center, Butwal, Rupandehi, Nepal
[5]Hydra Research and Policy Center, Kathmandu, Nepal
** Corresponding E-mail: gck223@gmail.com*

Received: *25 September, 2017;* ***Revised****: 28 October, 2017;* ***Accepted:*** *15 November, 2017*

ABSTRACT

The electronic structures and optical properties of pristine BiOBr and Cu, Ag and Au doped BiOBr have been analyzed by using a standard density functional theory based ab-initio approach employing generalized gradient approximation through revised Perdew Burke Ernzerhoff type parameterization. The calculation shows that both the doped and pristine BiOBr have indirect band gap, the band gap of the pristine BiOBr found 2.22eV, whereas band gap significantly reduced after doping Cu, Ag and Au on BiOBr. The band gap of Cu, Ag and Au doped BiOBr are 1.2eV, 0.9eV and 1.76eV respectively. The optical properties have been studied through dielectric function, both pure and doped BiOBr shows anisotropic nature.

Keywords: Density Functional Theory (DFT), BiOBr, Band structure, Density of State, Optical property, Doping.

INTRODUCTION

In the past few year, semiconductor based photocatalysts have developed as an effective compound for removing organic and inorganic component from water and air (Mills *et al.*, 1993; Hoffmann *et al.*,1995; Oliveros *et al.*, 1993; Carey *et al.*, 1976). Among semiconductor photocatalysts TiO_2 has received much focused , because of its strong oxidizing power, nontoxicity and cheapness (Ao *et al.*, 2004), however, very low amount of light is absorbed for photo degradation process due to its wide band gap (3.2 eV) (Liqiang *et al.*, 2002). Therefore, to increase the maximum utilization of electromagnetic wave (visible light) in order to boost photocatalytic activities, the improvement of semiconductor photocatalysts has developed as a vital issue in current photocatalysis research.

Pristine (Huang, 2009; Zhang, *et al.*, 2006; Wang *et al.*, 2009), doped (Miguel *et al.*, 2013; Jiahui *et al*. 2013) and co-doped (Jiang *et al.*, 2014 & 2015) bismuth oxyhalides preformed excellent photocatalytic activities because of its narrow band gap and outstanding photocatalytic performance and have become worthwhile candidate for research. Recently, BiOBr has appeared as new kind of visible light responsive photocatalysts and received much more interest from researcher, also made it as potential photocatalysts. Experimentally and theoretically large number of strategies have been developed to narrowing the band gap and boost the optical absorption of BiOBr, which includes doping metal (Li *et al.*, 2015) or co-doping of (Jiang *et al.*, 2014 & 2015), doping non-metal elements (Jiang *et al.*, 2014). As doping species, variable-valance metallic ions have been successive methods to narrowing band gap and enhancing the photocatalytic properties (Liu *et al.*, 2014). BiOBr has lamellar-structure and a p-type intrinsic semiconductor with indirect band gap to be in rang of 2.77-2.9 eV experimentally (Jiang *et al.*, 2010; Wang *et al.*, 2008) and 2.36 eV DFT calculation (Huang *et al.*, 2009). The wider band

gap (~2.9 eV) of BiOBr indicate that, only a part of the visible light could be absorb. The recent experimental work shows that, doping transition metal Ag, Al, Fe (Jiang *et al.*, 2013) and Ti (Wang *et al.*, 2012) on BiOBr narrow the band gap and increase the wavelength response rang to the visible region.

The present work focuses to engineer band structure of pristine BiOBr by doping transition metal X (Cu, Ag, and Au) and enhance the optical absorption near visible light range also examine the optical property through dielectric function analysis. Organization of this paper is as follows, next section discusses the method and computational details, followed by result and discussion section and conclusion of the work.

Computational details

Atomisitix Toolkit-Virtual Nanolab (ATK-VNL) has been used for the entire computational calculation, which is based on Density Functional Theory (DFT) (Kohn & Sham, 1965; Dreizler & Gross, 2012) and also includes non-equilibrium green function NEGF (Brandbyge *et al.*, 2002). ATK-VNL is based on the methodology, model, and algorithms development in academic code TransSIESTA and is further development of TransSIESTA-C (Stokbro *et al.*, 2003 and in part, McDcal (Taylor *et al.*, 2001), using localized basis sets as developed in SIESTA (Soler *et al.*, 2002). The generalized gradient approximation with revised Perdew Burke Eenernoff (Ying *et al.*, 2011; Perdew *et al.*, 1996) parameterization used as exchange correlation function. Double-ζ-double-polarized (DZDP) basis set used to describe valence electrons with localized pseudo atomic orbitals (PAOs) (Bachelet *et al.*, 1982). A mesh cut off of 75 Hartree is applied in entire calculation with maximum force tolerance set to 0.05eV/A and k-point sampling of 5×5×5. Before proceeding to further computational analysis, all the samples were freely optimized.

RESULTS AND DISCUSSION

Crystal Structure Analysis

In this section we discusses the crystal structure of pure BiOBr and X (Cu, Ag, Au) doped BiOBr before and after optimization. Here, we substituted X element at the place of Br on Pristine BiOBr. The optimized structures are given below.

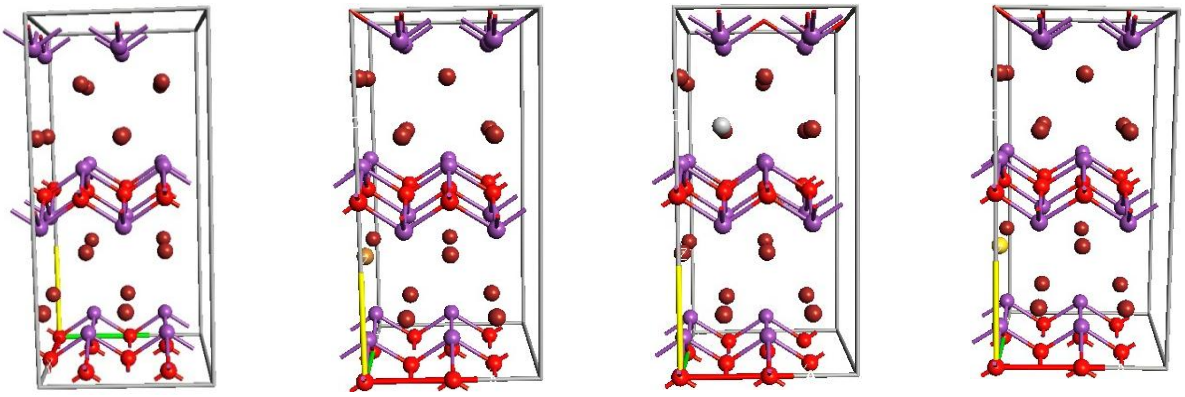

(a) (b) (c) (d)

Fig. 1. Optimized structure of (a) BiOBr (b) BiOBr-Cu (c) BiOBr-Ag (d) BiOBr-Au

Table 1: Angle and Bond lengths of Optimized Pure and doped BiOBr.

Structures	Angles				Bond length(Å)			
	Bi-O-Bi	O-Bi-O	O-Br-O	O-x-O	Bi-O	Br-Bi	Bi-X	Br-X
BiOBr	113.90	113.90	69.92	-	2.33	4.00	-	-
BiOBr-Cu	114.35	113.08	69.43	68.90	2.36	4.11	4.13	3.91
BiOBr-Ag	114.88	114.88	69.48	57.05	2.36	4.10	4.30	3.91
BiOBr-Au	114.24	113.37	69.37	55.51	2.32	4.10	3.98	3.91

As the transition metals are doped the bond angle increased for Bi-O-Bi. We can see that the bond angle of O-X-O is decreases with the growing X atomic number.

Electronic Band Structure

The energy difference on conduction band and valance band gives the energy band gap, here, on pure BiOBr valance band is due to the presence of O (2s, 2p) and Bi (6s), Br (4s, 4p) states whereas, conduction band consist mainly Bi (5d, 6p) and Br (4d) states. Our calculation shows an indirect band gap of 2.21 eV on BiOBr, which is agreeable with the earlier computational work (Huang *et al.*, 2009) and lower then experimental analysis (Wang *et al.*, 2008; Jiang *et al.*, 2010). Again the computed band gap of doped BiOBr-Cu is 1.2 eV, BiOBr-Ag is 0.9 eV and BiOBr-Au 1.76eV which are all indirect in nature. The band gap of pristine and doped BiOBr are given below.

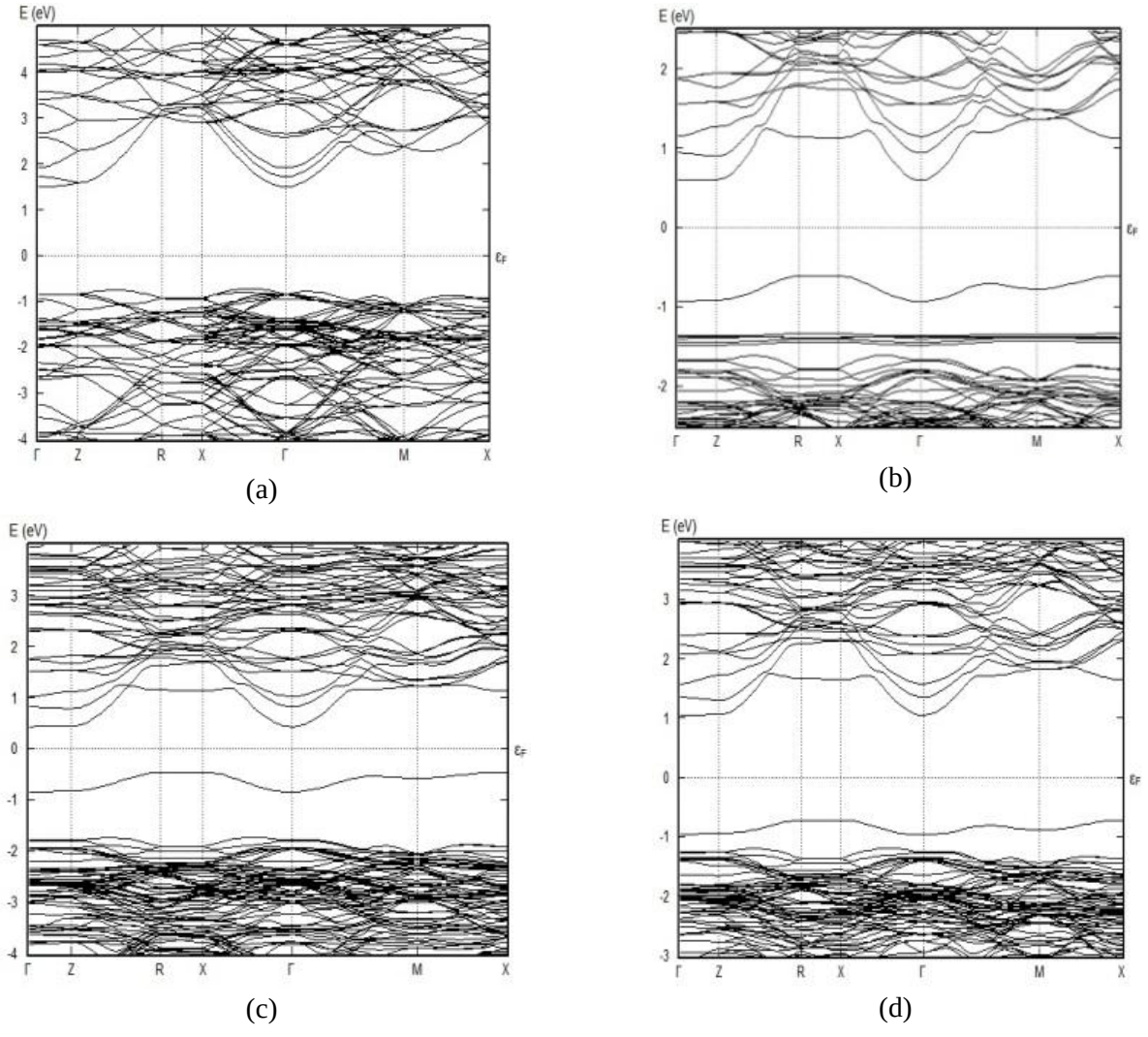

Fig. 2. Band Structure of (a) BiOBr, (b) BiOBr-Cu, (c) BiOBr-Ag, (d) BiOBr-Au

Here the band gap of the pure BiOBr is significantly reduced by doping group 11, transition metals X (Cu, Ag and Au). From above figure BiOBr valance band is fully occupied and consist mostly Br-4p and O-2p states, whereas Bi-6p state provides major contribution on empty conduction bands. From the above figure, a new impurity energy level appeared below the Fermi level on doped BiOBr. The X dopants (d-block elements) introduce an unpaired electron and upsurge asymmetry between the nearest atoms. The formation of impurity energy levels are because of delocalization of d states of X elements.

Our desire is that to reduce the band gap of pure BiOBr by doping transition metals and increase the

visible light absorption rate. The computed band gap of BiOBr is 2.22 eV, which say that it would absorb only a part of visible light. To get the excellence photocatalytic activity we must narrowing the band gap and X dopant elements successfully narrowed the energy.

Density of states

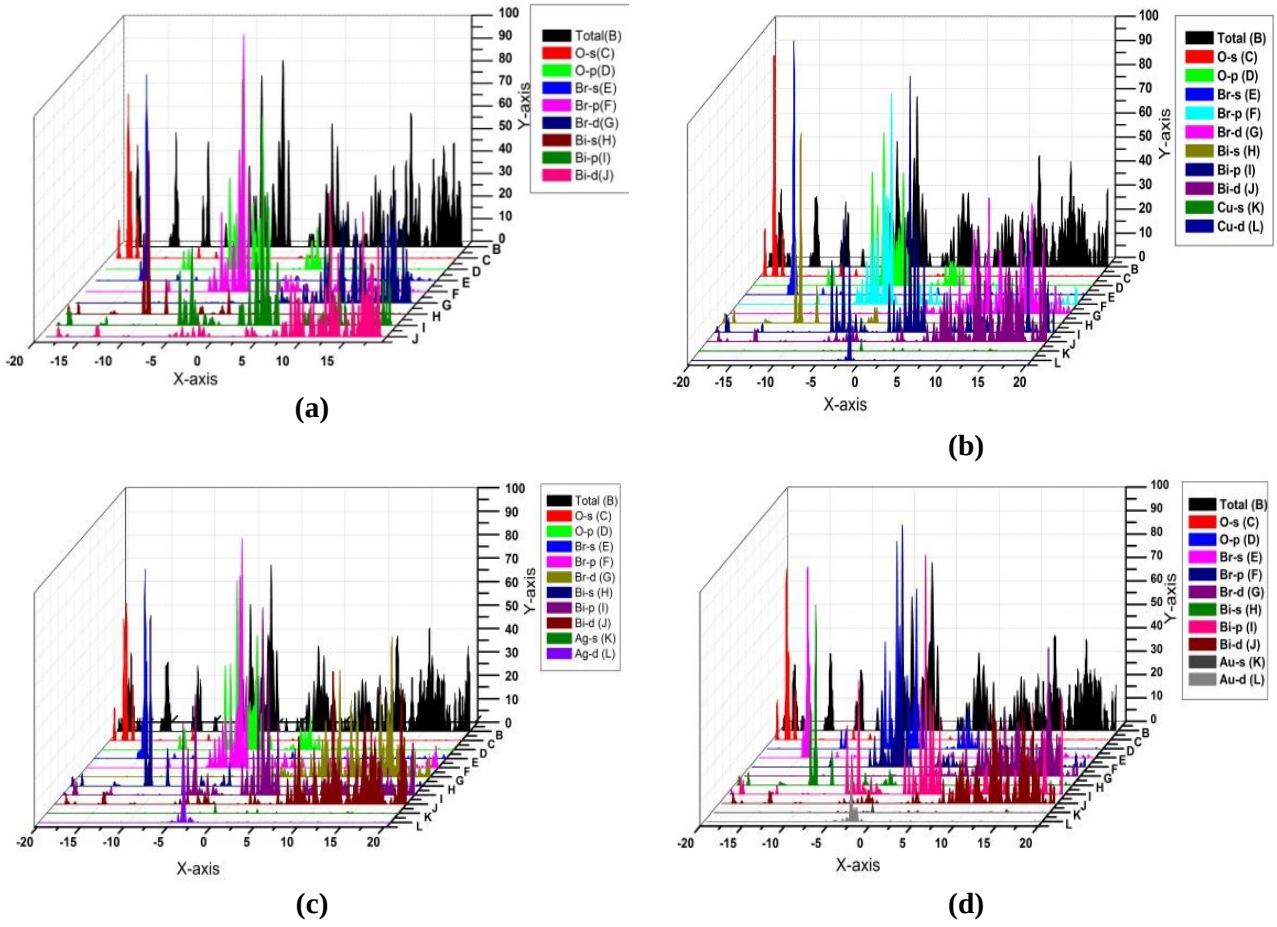

Figure 3: Total and partial DOS of (a) BiOBr, (b) BiOBr-Cu, (c) BiOBr-Ag and (d) BiOBr-Au.

The total (DOS) and partial density of states of (PDOS) of BiOBr and BiOBr-X is offered in figure 3. As we mention earlier and the figure analysis, Bi-6p, O-2p and Br-4p orbitals constitutes together both valance and conduction band, whereas O-2p and Br-4p orbitals mostly dominate the valance band and Bi-6p mostly dominate the conduction band in both structure, BiOBr and doped BiOBr. The conduction band is composed of Bi-5d, Br-4d, and valence band consist O-2s, Br-4s and Bi-6s orbitals. From the above figure 3, both d and s orbitals of X elements haven't any contribution on conduction band.

Pristine as well as doped structure of BiOBr, maximum peak observed at between -5.0 eV- 0 eV near Fermi level at valence band, is because of hybridization between O-2p and Br-4p states and doped X elements d-orbitals too. The fare most peaks on valance band are due to O-2s, Br-4s and Bi-6s states. Here, Bi-5d, 6p and Br-3d states hybridization leads the peaks on conduction band. The doped X elements d-state have peak near Fermi level at valence band, which gives support for the newly appeared impurity energy level at band structures on valance band, near Fermi level.

Optical spectrum

The complex dielectric function ε(ω) described the optical properties of matter, by observing the response of the system to electromagnetic wave (light). It can be expressed as

$$\varepsilon(\omega)=\varepsilon_1(\omega) + i\varepsilon_2(\omega) \quad (1)$$

Where $\varepsilon_1(\omega)$ is the real and $\varepsilon_2(\omega)$ is the imaginary part and can be analyzed through the Kramers-Krining dispersion relation.

There are two factor to account ε(ω), interband transitions and intraband transitions. An Intraband transition is only account for metals. There are also two types of transition on intaband transitions, direct and indirect transitions. The real and imaginary part of dielectric function of BiOBr doped structure along ε_{xx}, ε_{yy}, ε_{zz} polarizations is shown in figure 4.

Figure 4 indicates that, both real and imaginary part of dielectric function of BiOBr and doped BiOBr have maximum absorption values to the ε_{yy} direction.

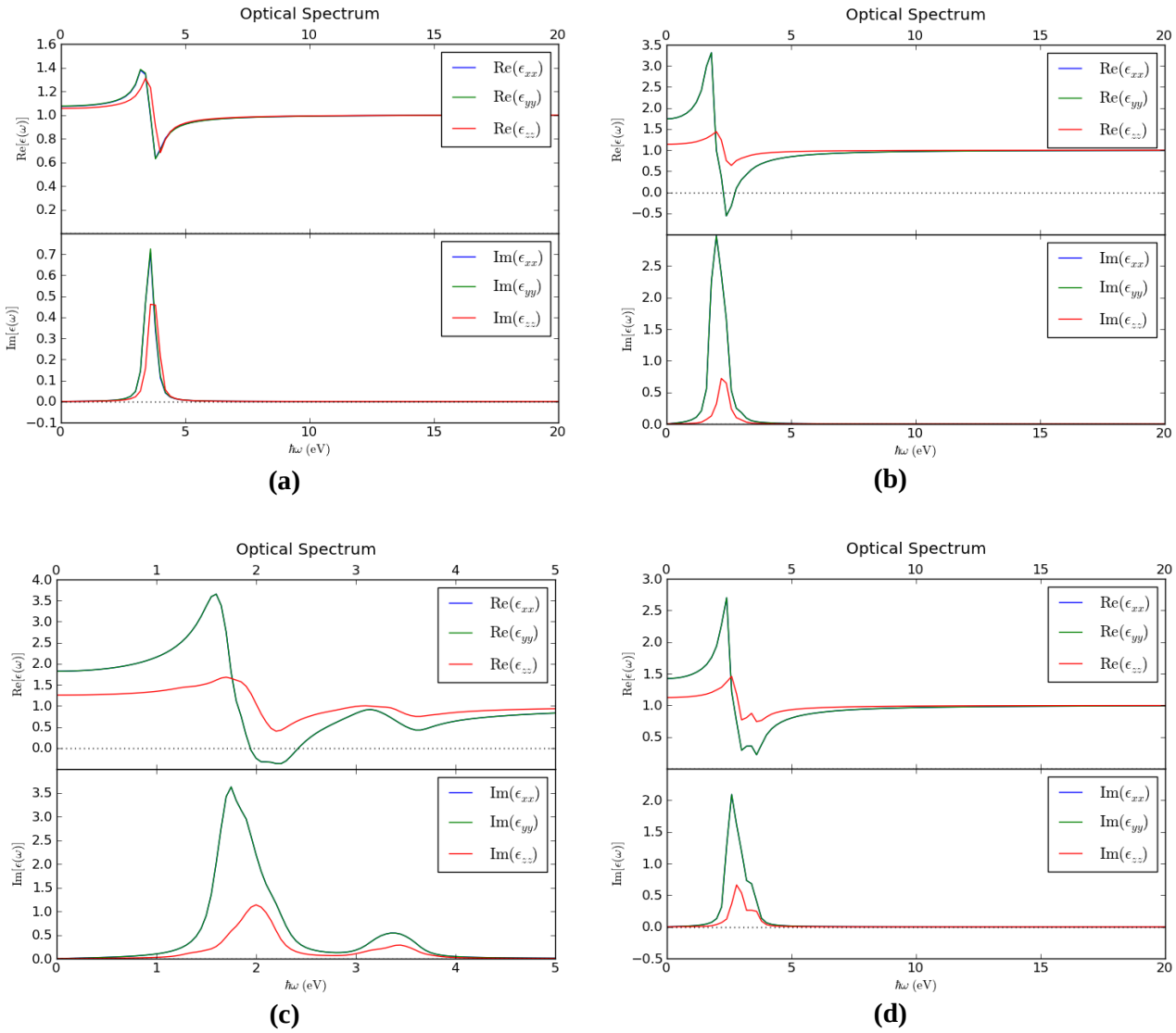

Fig. 4. Optical spectrums of (a) BiOBr, (b) BiOBr-Cu, (c) BiOBr-Ag and (d) BiOBr-Au

Table 2: Table showing the Real and Imaginary parts of dielectric functions.

Structure	ε_{xx} (Real)	ε_{yy} (Real)	ε_{zz} (Real)	ε_{xx} (Imaginary)	ε_{yy} (Imaginary)	ε_{zz} (Imaginary)
BiOBr	3.20	3.20	3.40	3.60	3.60	3.60
BiOBr-Cu	1.80	1.80	2.00	2.00	2.00	2.20
BiOBr-Ag	1.60	1.60	1.70	1.75	1.75	2.00
BiOBr-Au	2.40	2.40	2.60	2.60	2.60	2.80

Here, real part of dielectric function of BiOBr have maximum value at 3.20 eV, 3.40 eV; Cu-doped BiOBr have 1.8eV, 2.0eV; Ag-doped BiOBr have 1.6eV, 1.7eV and Au-doped BiOBr have 2.40eV, 2.60eV on ε_{yy} and ε_{zz} polarization direction respectively. Similarly for the imaginary part BiOBr have maximum value at 3.60eV, 3.60eV; Cu-doped BiOBr have 2.00eV, 2.20eV; Ag-doped BiOBr have 1.750eV, 2.0eV and Au-doped BiOBr have 2.60eV, 2.80eV on ε_{yy} and ε_{zz} polarization direction respectively. These peaks are raised because of the energy transition between orbitals corresponding to certain energy.

The imaginary part of dielectric function can be assigned the absorption peaks. As the photon energy is increased, the first peak links to the transition from the valence band to the conduction band. Here, the X elements introduced the d-orbitals, has a significant contribution on valence band. The peaks appeared on optical spectrum are similar to the peaks of DOS, on the presence of X element, the peaks got higher value in optical spectrum at low photon energy. The BiOBr-Ag structure has highest peak around 3.6 with lowest photon energy 1.60 eV and pure BiOBr has lowest peak at highest photon energy.

CONCLUSION

Electronic band structures, density of state and optical spectrum of pure and X doped BiOBr have been calculated, by using DFT based ab-initio approach. The electronic properties were studied via band structure and density of state. Wider band gap of BiOBr can be narrowed by doping X (Cu, Ag, and Au) elements. The doped structure claim themselves as a potential photocatalyst material due to their narrow band gap, among them BiOBr-Ag has narrow band gap and suitable candidate for photocatayst. The optical properties examined through dielectric function analysis and found that the maximum peaks appeared at BiOBr-Ag doped structure at lowest photon energy and lowest peaks appeared on BiOBr structure at highest photon energy. Both the pure and doped structures are anisotropic in nature.

ACKNOWLEDGMENT

The authors are thankful to ABV-IIITM, Gwalior for providing the infrastructural support to carry out the present research work. HRPC, Nepal is also acknowledged for partial support.

REFERENCES

Ao, C. H.; Lee, S. C.; Yu, J. Z. and Xu, J. H. (2004). Photodegradation of formaldehyde by photocatalyst TiO_2: effects on the presences of NO, SO_2 and VOCs. *Applied Catalysis B: Environmental,* **54** (1): 41-50.

AtomistixToolKitversion11.8.2 and 2014.2 Quantum Wise A/S. ⟨www.quantumwise.com⟩.

Bachelet, G. B.; Hamann, D. R. and Schlüter, M. (1982). Pseudopotentials that work: From H to Pu. *Physical Review B,* **26** (8): 4199.

Brandbyge, M.; Mozos, J. L.; Ordejón, P.; Taylor, J. and Stokbro, K. (2002). Density-functional method for nonequilibrium electron transport. *Physical Review B,* **65** (16): 165401.

Carey, J. H.; Lawrence, J. and Tosine, H. M. (1976). Photodechlorination of PCB's in the presence of titanium dioxide in aqueous suspensions. *Bulletin of Environmental Contamination and Toxicology,* **16** (6): 697-701.

Dreizler, R. M. and Gross, E. K. U. (2012). Density functional theory: an approach to the quantum many-body problem. *Springer Science & Business Media.*

Guerrero, M.; Pané, S.; Nelson, B. J.; Baró, M. D.; Roldán, M.; Sort; J. *et al.* (2013). 3D hierarchically porous Cu–BiOCl nanocomposite films: one-step electrochemical synthesis, structural characterization and nanomechanical and photoluminescent properties. *Nanoscale,* **5** (24): 12542-12550.

Hoffmann, M. R.; Martin, S. T.; Choi, W. and Bahnemann, D. W. (1995). Environmental applications of semiconductor photocatalysis. *Chemical reviews,* **95** (1): 69-96.

Huang, W. L. (2009). Electronic structures and optical properties of BiOX (X= F, Cl, Br, I) via DFT calculations. *Journal of computational chemistry,* **30** (12): 1882-1891.

Huang, W. L. and Qingshan, Z. (2009). DFT calculations on the electronic structures of BiOX (X= F, Cl, Br, I) photocatalysts with and without semicore Bi 5d states. *Journal of computational chemistry,* **30** (2): 183-190.

Jiang, G. H.; Li, X.; Wei, Z.; Jiang, T. T.; Du, X. X. and Chen W. X. (2015). Effects of N and/or

S Doping on Structure and Photocatalytic Properties of BiOBr Crystals. *Acta Metallurgica Sinica (English Letters)*, **28** (4): 460-466.

Jiang, G.; Li, X.; Wei, Z. Z. and Chen, W. (2014). Growth of N-doped BiOBr nanosheets on carbon fibers for photocatalytic degradation of organic pollutants under visible light irradiation. *Powder Technology*, **260**: 84-89.

Jiang, G.; Li, X.; Wei, Z. Z. and Chen, W. (2014). Immobilization of N, S-codoped BiOBr on glass fibers for photocatalytic degradation of rhodamine B. *Powder Technology*, **261**: 170-175.

Jiang, G.; Xiaohong, W.; Zhen, W.; Xia, L.; Xiaoguang, X.; Ruanbing, H. *et al.* (2013). Photocatalytic properties of hierarchical structures based on Fe-doped BiOBr hollow microspheres. *Journal of Materials Chemistry A*, **1** (7): 2406-2410.

Jiang, Z.; Yang, F.; Yang, G.; Kong, L.; Jones, M. O.; Xiao, T. *et al.* (2010). The hydrothermal synthesis of BiOBr flakes for visible-light-responsive photocatalytic degradation of methyl orange. *Journal of Photochemistry and Photobiology A: Chemistry*, **212** (1): 8-13.

Kohn, W. and Sham, L. J. (1965). Self-consistent equations including exchange and correlation effects. *Physical Review*, **140** (4A): A1133.

Li, X.; Mao, X.; Zhang, X.; Wang, Y.; Wang, Y.; Zhang, H.; *et al.* (2015). Citric acid-assisted synthesis of nano-Ag/BiOBr with enhanced photocatalytic activity. *Science China Chemistry*, **58** (3): 457-466.

Liqiang, J.; Xiaojun, S.; Jing, S.; Weimin, C.; Zili, X.; Yaoguo, D. *et al.* (2003). Review of surface photovoltage spectra of nano-sized semiconductor and its applications in heterogeneous photocatalysis. *Solar Energy Materials and Solar Cells*, **79** (2): 133-151.

Liu, Z.; Wu, B.; Zhao, Y.; Niu, J. and Zhu, Y. (2014). Solvothermal synthesis and photocatalytic activity of Al-doped BiOBr microspheres. *Ceramics International*, **40** (4): 5597-5603.

Mills, A.; Richard, H. D. and Worsley, D. (1993). Water purification by semiconductor photocatalysis. *Chem. Soc. Rev.*, **22** (6): 417-425.

Oliveros, L.; Oliveros, E. and Braun, A. M. (1993). Photochemical processes for water treatment. *Chemical Reviews*, **93** (2): 671-698.

Perdew, J. P.; Burke, K. and Ernzerhof, M. (1996). Generalized gradient approximation made simple. *Physical review letters*, **77** (18): 3865.

Soler, J. M.; Emilio, A.; Julian, D. G.; Alberto G.; Javier, J.; Ordejón, P. *et al.* (2002). The SIESTA method for ab initio order-N materials simulation. *Journal of Physics: Condensed Matter*, **14** (11): 2745.

Stokbro, K.; Taylor, J.; Brandbyge, M. and Ordejon, P. (2003). TranSIESTA: a spice for molecular electronics. *Annals of the New York Academy of Sciences*, **1006** (1): 212-226.

Taylor, J.; Hong, G. and Jian, W. (2001). Ab initio modeling of quantum transport properties of molecular electronic devices. *Physical Review B*, **63** (24): 245407.

Wang, R.; Guohua, J.; Xiaohong, W.; Ruanbing, H.; Xiaoguang, X.; Shiyong, B. *et al*. (2012). Efficient visible-light-induced photocatalytic activity over the novel Ti-doped BiOBr microspheres. *Powder Technology*, **228**: 258-263.

Wang, W.; Fuqiang, H.; Xinping, L. and Jianhua, Y. (2008). Visible-light-responsive photo-catalysts xBiOBr–(1−x) BiOI. *Catalysis Communications*, **9** (1): 8-12.

Wang, W.; Huang, F.; Lin, X. and Yang, J. (2008). Visible-light-responsive photocatalysts xBiOBr–(1−x) BiOI. *Catalysis Communi-cations*, **9** (1): 8-12.

Ying, W.; Lai, Y. and Zhang, Z. Q. (2011). Elastic metamaterials with simultaneously negative effective shear modulus and mass density. *Physical review letters*, **107** (10): 105506.

Yu, J.; Wei, B.; Zhu, L. and Xu, L. (2013). Flowerlike C-doped BiOCl nanostructures: Facile wet chemical fabrication and enhanced UV photocatalytic properties. *Applied Surface Science*, **284**: 497-502.

Zhang, K. L.; Liu, C.; Huang, F. Q. and Wang, W. D. (2006). Study of the electronic structure and photocatalytic activity of the BiOCl photocatalyst. *Applied Catalysis B: Environmental*, **68** (3): 125-129.